Bioactive Materials 11 (2022) 130–139

Contents lists available at ScienceDirect

Bioactive Materials

journal homepage: www.keaipublishing.com/en/journals/bioactive-materials

Facile fabrication of a biocompatible composite gel with sustained release of aspirin for bone regeneration

Yunfan Zhang [a,b], Xueyu Dou [c,d], Lingyun Zhang [a,b], Hufei Wang [c,d], Ting Zhang [a,b], Rushui Bai [a,b], Qiannan Sun [a,b], Xing Wang [c,d,*], Tingting Yu [a,b,**], Decheng Wu [c,d], Bing Han [a,b,***], Xuliang Deng [b,e]

[a] Department of Orthodontics, Peking University School and Hospital of Stomatology, Beijing, PR China
[b] National Center of Stomatology, National Clinical Research Center for Oral Diseases, National Engineering Laboratory for Digital and Material Technology of Stomatology, Beijing Key Laboratory for Digital Stomatology, Research Center of Engineering and Technology for Computerized Dentistry Ministry of Health, NMPA Key Laboratory for Dental Materials, Beijing, PR China
[c] Beijing National Laboratory for Molecular Sciences, Institute of Chemistry, Chinese Academy of Sciences, Beijing, PR China
[d] University of Chinese Academy of Sciences, Beijing, PR China
[e] Department of Geriatric Dentistry, Peking University School and Hospital of Stomatology, Beijing, PR China

ARTICLE INFO

Keywords:
Hydrogel
Aspirin
Chitosan
Drug sustained-release
Bone tissue engineering

ABSTRACT

Hydrogels are extracellular-matrix-like biomimetic materials that have wide biomedical applications in tissue engineering and drug delivery. However, most hydrogels cannot simultaneously fulfill the mechanical and cell compatibility requirements. In the present study, we prepared a semi-interpenetrating network composite gel (CG) by incorporating short chain chitosan (CS) into a covalent tetra-armed poly(ethylene glycol) network. In addition to satisfying physicochemical, mechanics, biocompatibility, and cell affinity requirements, this CG easily encapsulated acetylsalicylic acid (ASA) *via* electrostatic interactions and chain entanglement, achieving sustained release for over 14 days and thus promoting periodontal ligament stem cell (PDLSC) proliferation and osteogenic differentiation. *In vivo* studies corroborated the capacity of PDLSCs and ASA-laden CG to enhance new bone regeneration *in situ* using a mouse calvarial bone defect model. This might be attributed to PDLSCs and host mesenchymal stem cells expressing monocyte chemoattractant protein-1, which upregulated M2 macrophage recruitment and polarization *in situ*, indicating its appealing potential in bone tissue engineering.

1. Introduction

Critical-sized bone defects secondary to trauma, infection, congenital bone disease, or tumor resection cannot be reconstructed without intervention, representing a clinical and public health issue worldwide [1–3]. Conventional materials for bone defect repair include autografts, allografts, or bone substitutes. Although autologous bone grafting remains the gold standard among therapeutic strategies, limited donor tissue and excessive surgery risks are still major concerns [4,5]. Allogeneic or xenogeneic bone grafting might give rise to *de novo* problems, including immune rejection and pathogen transmission [1,6]. Fortunately, bone regeneration *via* artificially designed and synthesized biomimetic scaffolds has emerged as a new technique to fulfill this demand. Cell-based strategies have proven to be promising alternatives in tissue engineering and regenerative medicine (TERM). With the advances in exogenous progenitor cell selection, design strategies of bionic scaffolds based on the loading and spatiotemporally-disciplined release of bioactive factors has become a promising approach in bone tissue engineering (BTE) to reconstruct critical bone defects.

The immune system plays key roles in bone homeostasis, and aberrant osteoimmune microenvironments during bone healing and BTE might lead to less neo-bone formation and poorer repair outcomes [7,8]. Among immune cells, macrophages, the major producers of cytokines, are recruited to bone defect areas, where they determine local reactions

Peer review under responsibility of KeAi Communications Co., Ltd.
* Corresponding author. Beijing National Laboratory for Molecular Sciences, Institute of Chemistry, Chinese Academy of Sciences, Beijing, 100190, PR China.
** Corresponding author. Department of Orthodontics, Peking University School and Hospital of Stomatology, Beijing, 100081, PR China.
*** Corresponding author. Department of Orthodontics, Peking University School and Hospital of Stomatology, Beijing, 100081, PR China.
E-mail addresses: wangxing@iccas.ac.cn (X. Wang), tingtingyu@bjmu.edu.cn (T. Yu), kqbinghan@bjmu.edu.cn (B. Han).

https://doi.org/10.1016/j.bioactmat.2021.09.033
Received 14 July 2021; Received in revised form 24 September 2021; Accepted 28 September 2021
Available online 5 October 2021
2452-199X/© 2021 The Authors. Publishing services by Elsevier B.V. on behalf of KeAi Communications Co. Ltd. This is an open access article under the CC BY-NC-ND license (http://creativecommons.org/licenses/by-nc-nd/4.0/).

towards bioactive scaffolds over the long term [9,10]. In addition, macrophages polarized to the M2 phenotype are believed to promote tissue healing and mesenchymal stem cell (MSC) osteogenesis [11,12]. The emerging concept of the immunomodulation capacity of biomaterials has been applied to bone regeneration applications [11,13]. Various modification strategies to achieve local sustained release of immunomodulatory agents, including non-steroidal anti-inflammatory drugs (NSAIDs) or appropriate surface nano-topography design, have been investigated. Acetylsalicylic acid (ASA), also known as aspirin, can promote bone regeneration. Numerous articles have elaborated its underlying mechanisms, most of which are related to osteo-immunomodulation, including T cell suppression, elongation of MSC life span, and upregulation of immunomodulation capacity [14–17]. Periodontal ligament stem cells (PDLSCs) were separated as novel dental MSCs in 2004 [18]. Studies reported that PDLSCs possess superior proliferation, differentiation, and immunomodulation abilities [19], making them appealing candidate seed cells for BTE. Recent developments in tissue engineering have led to increased interest in enhancing structural and compositional components of scaffolds. Accordingly, extensive studies have determined the significance of three-dimensional (3D) constructs, namely their morphological resemblance to the structure of the native extracellular matrix (ECM). Hydrogels, natural 3D polymeric materials, have many unique properties, including high porosity, high water retention capacity, and diverse physical properties of natural tissue that enable them to mimic the natural ECM, and thus can be applied in tissue engineering [20–22]. However, they possess some inherent disadvantages, such as a delicate nature, poor mechanical strength, or a premature degradation profile because of structural defects, especially their swollen state *in vivo*, which greatly limits their applicability.

In general, hydrogels are prepared from either synthetic or natural polymers. Although many approaches have been developed to improve their mechanical properties, most synthetic hydrogels cannot fulfill the cell-compatibility requirements of biomedical applications. For example, tetra-armed poly(ethylene glycol) (tetra-PEG) hydrogels possessed uniform networks and favorable mechanical properties [23]. However, cell adhesion, proliferation, and growth were unsatisfactory, which has limited their applications in tissue engineering. In contrast, natural polymers involving alginate, chitosan, hyaluronic acids, and collagen have greater inherent biocompatibility and desirable biodegradability, representing promising bone tissue regenerative biomaterials for clinical use [24]; however, their undesirable mechanical strength is a challenge. Among these natural hydrogel materials, chitosan (CS) is an excellent candidate for potential drug delivery and tissue engineering [25,26], because this cationic copolymer is hydrophilic in nature and is enzymatically degradable. In addition, CS is the only alkaline polysaccharide with physical chain-entanglement network and a number of natural amino groups that could generate electrostatic interactions with carboxyl-modified drugs or bioactive factors to contribute to controlled drug release behaviors [27]. Nevertheless, a CS physical network is not usually the preferred choice to build high-performance hydrogels because of its low solubility and the high viscosity of long-chain CS, which could result in brittle hydrogel scaffolds [28].

To simultaneously fulfill the mechanical and cell-compatible requirements of biomedical applications, in the present study, we integrated short-chain CS (high solubility in neutral water) into a covalent tetra-PEG network via hydrogen bonding to construct a tetra-PEG-CS composite gel (CG). The uniform backbone of the tetra-PEG network provided high mechanical strength and the CS components benefited PDLSC adhesion, thus acquiring simultaneous favorable mechanical properties and cell growth abilities. This biocompatible tetra-PEG-CS hydrogel could bind ASA molecules *via* electrostatic interactions and polymeric chain entanglement. The suitable pore structure, swelling ratio, and degradation time, meant that ASA molecules could be released in a sustained manner from the biodegradable ASA-encapsulated tetra-PEG-CS composite gel (CG-ASA) over 2 weeks, thus effectively enhancing PDLSC osteogenic differentiation *in vitro*. After *in vivo* implantation for 8 weeks, this non-toxic, bioactive, and mechanically and functionally optimized CG-ASA combined with PDLSCs promoted significant bone tissue regeneration, as assessed using histological tests, micro-computed tomography (CT), specific markers analysis, and bone mass measurements. The underlying mechanism of CG-mediated bone regeneration might be associated with MCP-1 secretion and M2 macrophage recruitment and polarization.

2. Materials and methods

2.1. Materials

Tetra-PEG-NH_2 (M_W = 10 kDa) and Tetra-PEG succinimidyl carbonate (SC, M_W = 10 kDa) were purchased from SINOPEG (Xiamen, China). Chitosan was purchased from Jinhu Limited (Shandong, China). Aspirin was purchased from Sigma-Aldrich (St. Louis, MO, USA). Infrared (IR) grade potassium bromide was purchased from Aladdin (Shanghai, China). Ethanol, isopropanol, chloroform, and glutaraldehyde were purchased from Beijing Chemworks (Beijing, China). Six week old female C57BL6 mice were purchased from Vital River Laboratories (Beijing, China).

2.2. PDLSC isolation and identification

The primary cell isolation protocol was approved by the Peking University School of Stomatology Institutional Review Board (PKUSSIRB-201311103). Human donors aged 18–25 years old who claimed to have no history of periodontitis nor caries were included. Then, PDLSC isolation procedures were performed according to a previous publication [18]. Passage 3 (P3) cells were used for flow cytometric analysis. P3–P5 PDLSCs were used in the subsequent experiments.

2.3. PDLSC culture and osteogenic induction

The PDLSC Growth Medium (GM) comprised α-modified Eagle's medium (α-MEM, Gibco, Grand Island, NY, USA) supplemented with 15% fetal bovine serum (FBS, ABWbio, Shanghai, China), 1% penicillin/streptomycin (Solarbio, Beijing, China) and 2 mM glutamine (Gibco). Cells were cultured at 37 °C in 5% humidified CO_2. When the cell confluence reached 70–80%, the medium was replaced with PDLSC Osteogenic Differentiation Medium (ODM). ODM contains α-MEM, 15% FBS, 1% penicillin/streptomycin, 0.01 μM dexamethasone sodium phosphate, 1.8 mM KH_2PO_4, 0.1 mM L-ascorbic acid phosphate (Sigma-Aldrich), and 2 mM glutamine. Apart from the negative control (NC) group, the culture medium of the other groups in the *ex vivo* osteogenesis assay were based on ODM.

2.4. Alkaline phosphatase (ALP) staining

After 7-days of osteogenic induction, PDLSCs were fixed using 4% of paraformaldehyde (PFA) at ambient temperature for 15 min and then rinsed with phosphate-buffered saline (PBS) three times. A 5-bromo-4-chloro-3-indolyl phosphate (BCIP)/nitro blue tetrazolium (NBT) Kit (CWBIO, Beijing, China) was applied according to the manufacturer's protocol. Briefly, PDLSCs were stained using BCIP/NBT dyes in the dark for 30 min. After rinsing with PBS three times, the cells were viewed under a microscope, and ImageJ2 software (NIH, Bethesda, MD, USA) was used to measure the stained areas semi-quantitatively(n = 6).

2.5. Alizarin Red S (ARS) staining

After 14-days of osteogenic induction, PDLSCs were fixed and rinsed in the same way as ALP staining. PDLSCs were stained with 1% of ARS (Sigma-Aldrich) dye for 15 min at room temperature and then rinsed

with PBS three times. Stained PDLSCs were air-dried and photographed. ImageJ2 was used to measure the stained areas semi-quantitatively (n = 6).

2.6. Quantitative real-time reverse transcription PCR (qRT-PCR)

Total RNA extraction was conducted following the manufacturer's protocol using the TRIzol Reagent (Invitrogen, Waltham, MA, USA). The RNA concentration was determined using a NanoDrop 8000 spectrophotometer (Nanodrop Technologies, Wilmington, DE, USA). Total RNA (1 μg per sample) was reverse-transcribed to cDNA using ReverTra ACE qPCR RT Master Mix (TOYOBO, Osaka, Japan) following manufacturer's protocol. The cDNA was used as a template in a qPCR reaction, performed using FastStart Universal SYBR Green Master (Roche, Basel, Switzerland) on an ABI Prism 7500 Real-Time PCR System (Applied Biosystem, Foster City, CA, USA). Target gene expression was normalized to that of *GAPDH* (encoding glyceraldehyde-3-phosphate dehydrogenase). The result was analyzed using the $2^{(-\Delta\Delta CT)}$ method [29] (n = 6). The primer sequences are listed in Table 1.

2.7. Preparation of the ASA-Encapsulated tetra-PEG-CS composite gel (CG-ASA)

All solutions were prepared in ultra-pure water at room temperature. Chitosan (6 wt%) and ASA (200 μg/mL) were jointly dissolved in the same sample bottle, precursor molecules of tetra-PEG-NH_2 (15 wt%) were then added into the CS-ASA solution. An equivalent volume of tetra-PEG-SC solution (15 wt%) was added to the CS-ASA-tetra-PEG-NH_2 solution. The solution was thoroughly mixed *via* vortexing and then stood at room temperature to allow gelation. ASA was not required for the pure CG.

2.8. Scanning Electrical microscopy (SEM)

Briefly, the CG samples were fixed using 2.5% glutaraldehyde, gradient ethanol dehydrated, and lyophilized for SEM (Hitachi, Tokyo. Japan) observation. SEM images of CG (n = 3) and CG-ASA (n = 3) were acquired, and 8 pores in each image were selected randomly and measured.

2.9. Flourier transform infrared spectroscopy (FT-IR)

A small amount of CS powder and freeze-dried gels were mixed with IR-grade potassium bromide, ground to a fine powder, dried, and compacted into disks. In the range of 4000–400 cm^{-1} wavenumbers, 32 scans were carried out with a resolution of 2 cm^{-1} using FT-IR (Bruker, Karlsruhe, Germany).

2.10. Porosity

The porosity of freeze-dried CG was measured using the ethanol displacement method: 1) The initial weight, W_0, and volume, V_0, of the samples were measured. 2) CG samples were immersed in absolute ethanol for 2 min. 3) The residual ethanol on the surface of the samples as wiped off and the weight was recorded (W_1). The density of ethanol was marked as ρ. The porosity (%) of the samples was calculated using the following formula (n = 6):

$$Porosity\ (\%) = \frac{W_1 - W_0}{\rho V_0} \times 100\% \quad (1)$$

Table 1
Primer sequences of target genes for qPCR.

Gene	Forward (5′-3′)	Reverse (3′-5′)
GAPDH	GGAGCGAGATCCCTCCAAAAT	GGCTGTTGTCATACTTCTCATGG
RUNX2	TGGTTACTGTCATGGCGGGTA	TCTCAGATCGTTGAACCTTGCTA
ALP [30]	AACATCAGGGACATTGACGTG	GTATCTCGGTTTGAAGCTCTTCC
OCN	CACTCCTCGCCCTATTGGC	CCCTCCTGCTTGGACACAAAG
MCP-1	TTTCCAGATGCAATCAATGCC	TGGAATCCTGAACCCACTTCT

2.11. Swelling and degradation ratios

The initial weight, W_0, of freeze-dried CG samples was recorded. Then, samples were immersed in PBS at 37 °C, and the PBS was replaced every 2 days. In the swelling study, CGs were weighed after 0.25, 0.5, 1, 2, 4, 8, 12, 24, 48, 72, 96, and 120 h, and their weights were recorded as W_t. The swelling ratio (%) of the samples was calculated using following formula (n = 6):

$$Swelling\ Ratio\ (\%) = \frac{W_t - W_0}{W_0} \times 100\% \quad (2)$$

In the degradation study, CGs were rinsed, lyophilized, and weighed after 0 (W_0), 1, 4, 7, 14, 21, 28, 35, and 42 days, and the weights were recorded as W_t. The degradation ratio (%) of the samples was calculated using the following formula (n = 6):

$$Degradation\ Ratio\ (\%) = \frac{W_0 - W_t}{W_0} \times 100\% \quad (3)$$

2.12. Compression stress

CG (n = 6) and CG-ASA (n = 6) were prepared in a container with a diameter of 15 mm and a height of 6 mm. The samples were tested by Universal Testing Systems (Instron, MA, USA) at a compression rate of 3 mm/min.

2.13. In vitro ASA release

ASA-laden CGs (n = 6) were immersed in PBS at 37 °C. After 0.5, 1, 2, 3, 4, 5, 6, 7, 8, 10, 12, and 14 days of incubation, ASA-containing PBS was collected and the ASA concentrations were determined using high performance liquid chromatography (HPLC).

2.14. Cytotoxicity assays

Cell Counting Kit-8 (CCK-8) (Dojindo, Kumamoto, Japan) assays (n = 6) were applied following manufacturer's protocol. PDLSCs were seeded in a 48-well plate at 1×10^4 cells per well. After incubation for 24 h, GM, CG extract GM, with or without 100 μg/mL of ASA, was replaced in the NC, CG-ASA, and CG groups, respectively, for further incubation. OD values (450 nm) of the experimental group, NC group, and background were recorded as OD_E, OD_{NC} and OD_B, respectively. Cell viability (%) was defined using the following formula:

$$Cell\ Viability\ (\%) = \frac{OD_E - OD_B}{OD_{NC} - OD_B} \times 100\% \quad (4)$$

Live/dead staining was performed using a Live/Dead Viability/Cytotoxicity Kit (Invitrogen). PDLSCs were seeded and incubated with GM, and CG extract GM with or without 100 μg/mL of ASA (n = 6). Medium was replaced every 2 days. Fluorescence microscopy (Olympus, Tokyo, Japan) was used to observe the green and red fluorescence.

2.15. In vivo osteogenesis study of PDLSC-Loaded CG complexes

Freeze-dried CGs with diameter of 5 mm and height of 2 mm were disinfected using UV light. A suspension containing 2×10^5 PDLSCs was seeded into the CGs and incubated for 2 days to obtain the PDLSC-CG complexes. CGs without PDLSCs were immersed in GM and incubated for 2 days. Materials were cut into a diameter of 3 mm and height of 1–2 mm before surgery. The animal experiments were approved by Peking University Biomedical Ethics Committee (approval number LA2019074). Briefly, 8-week-old female C57BL6 mice were

anaesthetized. The surgery fields were shaved and disinfected. Then, 3 mm of full-thickness circular defects [31] were made in the center of mouse calvaria bone using a stainless-steel trephine. Mice were randomly divided into five groups for implantation: 1) NC group (n = 12), the defects were left unfilled; 2) CG group (n = 12), the defects were filled by CG; 3) PDLSC + CG group (n = 12), the defects were filled with PDLSC-laden CG; 4) CG-ASA group (n = 12), the defects were filled with CG-ASA, and 5) PDLSC + CG-ASA group (n = 12), the defects were filled with PDLSC-laden CG-ASA. Skin incisions were closed using 5-0 sutures. Mice were euthanized at 2 weeks (for macrophage and osteogenic marker immunohistochemistry staining [32], n = 6 in each group) and 8 weeks (for hematoxylin and eosin (H&E) staining, Masson staining, n = 6 in each group) after surgery, at which point, the calvarial bones were harvested and fixed with 4% PFA.

2.16. Micro-CT scanning and analysis

The calvarial bone specimens were scanned using an Invest MM Ganstry-Std CT (Siemens, Munich, Germany), at 80 kV and 500 μA. The bone volume/total volume (BV/TV) ratio was calculated using Inveon Research Workplace 3.0 (Siemens).

2.17. Histological staining

Briefly, the specimens were decalcified, dehydrated, and embedded. 4 μm thick serial sections were prepared and stained with H&E and Masson Staining Kits (Solarbio) to evaluate bone formation.

2.18. Enzyme-linked immunosorbent assay (ELISA)

Tetra-PEG hydrogel and CG extract GM were used to treat PDLSCs (n = 6). After incubation for 1, 4, and 7 days, the supernatant was collected. The levels of monocyte chemoattractant protein-1 (MCP-1) in the supernatant were detected using an MCP-1 ELISA Kit (MEIMIAN, Jiangsu, China) following manufacturer's protocol.

2.19. Immunohistochemistry (IHC)

Briefly, after routine dewaxing and hydrating, the sections were treated with proteinase K and trypsin mixed antigen retrieval solution for 30 min at 37 °C. Then, 5% of BSA was used to block non-specific binding. Primary antibodies against pan macrophage markers F4/80 (Cat. sc377009, 200 μg/mL, Santa Cruz Biotechnology, Santa Cruz, CA, USA), M1 macrophage marker inducible nitric oxide synthase (iNOS, Cat. 18985-1-AP, 1000 μg/mL, Proteintech Group, Rosemont, IL, USA), M2 macrophage marker CD206 (Cat. 18704-1-AP, 700 μg/mL, Proteintech Group), MCP-1 (Cat. ab25124, 1000 μg/mL, Abcam, Cambridge, UK) and RUNX2 (Cat. sc101145, 100 μg/mL, Santa Cruz Biotechnology) were added to the sections at 1:100 dilution at 4 °C overnight. After rinsing three times with PBS, the sections were incubated with corresponding horseradish peroxidase-conjugated secondary antibodies (Cat. ZB2301, ZB2305, 200 μg/mL, ZSGB Biotechnology, Beijing, China) at 1:5000 dilution or IHC enhanced polymer detection system (Cat. PV8000, ZSGB Biotechnology). Experiments were carried out following manufacturer's protocols (ZSGB Biotechnology). The samples were observed under optical microscopy (Zeiss, Wetzlar, Germany).

2.20. Statistics analysis

All the data were analyzed using SPSS 24.0 (IBM Corp., Armonk, NY, USA) and presented as the mean ± standard deviation (SD). Unpaired Student's t-tests and one-way analysis of variance (ANOVA) were applied for the statistical analysis.

3. Results

3.1. Preparation and characterization of CG-ASA scaffolds

A schematic illustration of the synthesis of the CG-ASA scaffolds is shown in Fig. 1. According to the intrinsic properties of the ammonolysis reaction between the amine and active ester groups, a strong covalent primary network of tetra-PEG was quickly formed, while the CS chains interacted with tetra-PEG network via chain-entanglement and hydrogen bonding. Some ASA molecules were distributed around the CS chains via electrostatic interactions, thus indicating the sustained-release behavior to prolong the maintenance time of an effective drug concentration *in situ*.

The optimal ASA loading concentration was determined *via in vitro* a PDLSC osteogenic differentiation assay. After being verified by flow cytometric analysis (Fig. S1A), PDLSCs were osteogenically induced using ODM supplemented with gradient concentrations of ASA for 7 or 14 days. ALP and ARS staining unanimously demonstrated that aspirin promoted osteogenesis in a dose-dependent manner. When the concentration was set at 100 μg/mL, ASA exhibited the greatest osteogenic induction of PDLSCs (Fig. S1B). Thus, we encapsulated ASA at a concentration of 100 μg/mL in CG-ASA (Fig. 2A). Empty CG and CG-ASA appeared to be semitransparent faint yellow under gross observation, resulting from CS integration (Fig. 2B). Absorbance peaks of the tetra-PEG hydrogel, CS, and CG were determined using by FT-IR (Fig. 2C). The wide peaks at 3429 cm^{-1} were associated with N–H and O–H stretching vibration and the signal of 2880 cm^{-1} was ascribed to C–H stretching vibration. In the spectrum of CS, 1080 cm^{-1} and 1157 cm^{-1} were the vibration peaks of pyranose. The existence of hydrogen bonds meant that the stretching vibration of C═O in the residual acetyl group of CS was located at 1610 cm^{-1}, and the bending vibration of N–H of the primary amine was located at 1512 cm^{-1}. In the spectra of tetra-PEG, absorbance peaks at 1662 cm^{-1} and 1117 cm^{-1} were related to amide I band and C–O–C vibration, but these two bands were shifted to 1637 cm^{-1} and 1113 cm^{-1} in the spectra of CG, which might be ascribed to the physical chain-entanglement and hydrogen bonds between tetra-PEG and CS chains. The peak at 1539 cm^{-1} corresponded to N–H bending vibration, confirming the existence of free amino groups of CS. SEM revealed the inner porous structure of CG and CG-ASA (Fig. 2D). Scaffolds with a suitable pore size and porosity enable host cell infiltration, as well as the exchange of nutrition and metabolic waste. The pore size and porosity of CG and CG-ASA were 85.1 ± 3.94 μm and

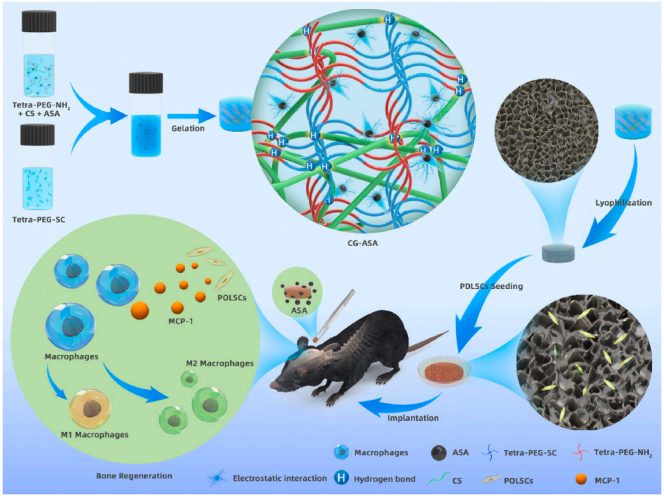

Fig. 1. Schematic illustration of the fabrication procedures of an acetylsalicylic acid (ASA)-encapsulated composite gel (CG-ASA) for mice calvaria bone defect regeneration. The underlying mechanism of CG-mediated bone regeneration might be ascribed to macrophage recruitment and M2 polarization.

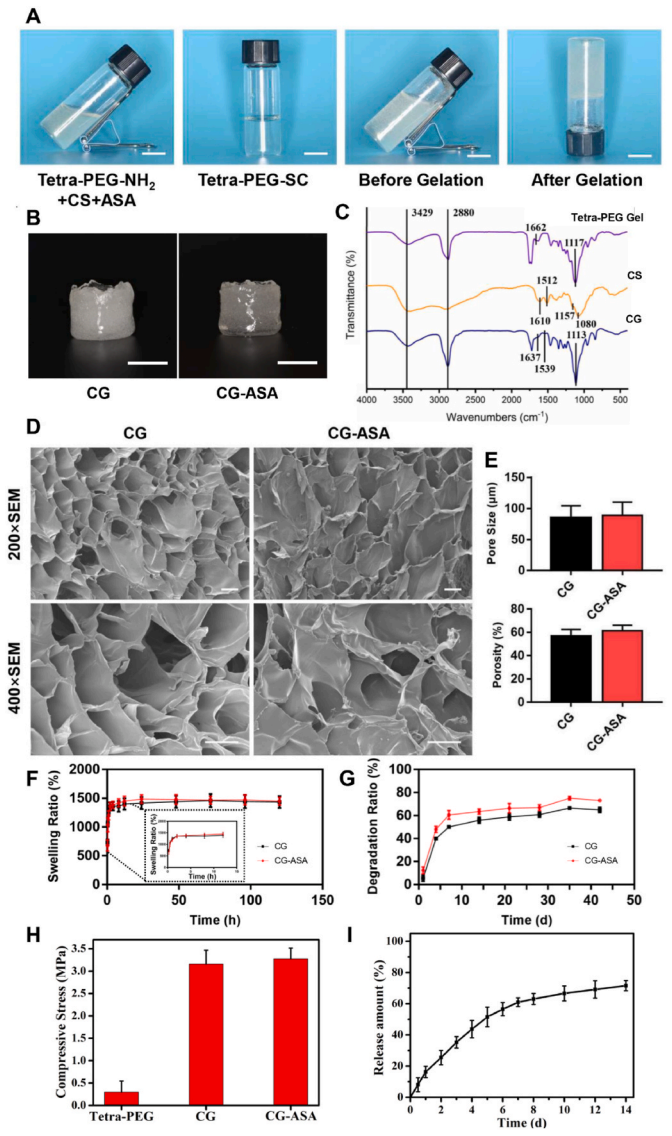

Fig. 2. Fabrication and characterization of CG and CG-ASA. (A) Synthesis procedures for CG-ASA. (B) Gross view of CG and CG-ASA, scale bar = 1 cm. (C) FT-IR spectra of tetra-PEG hydrogel, chitosan, and CG. (D) SEM images of the inner porous structure of CG and CG-ASA, scale bar = 50 μm. (E) Pore size and porosity, (F) Swelling, (G) Degradation profiles, and (H) compressive stress of CGs, with or without ASA loading. (I) ASA cumulative release curve of CG-ASA. CG, composite gel; ASA, acetylsalicylic acid; CG-ASA, ASA-encapsulated CG; FT-IR, Fourier transform infrared spectroscopy; PEG, polyethylene glycol; SEM, scanning electron microscopy.

57.05 ± 3.12%; and 89.0 ± 4.31 μm and 61.43 ± 2.75%, respectively (Fig. 2E). No significant difference was found between the two groups. The swelling and degradation profiles of hydrogels, particularly tissue engineering scaffolds, are important physical and biological properties to maintain the stability of scaffolds and promote neo-tissue regeneration. The swelling profiles showed that after immersion for 24 h in PBS, both CG and CG-ASA reached the equilibrium swelling state, and the swelling ratios at 120 h were 1436 ± 59.85% and 1449 ± 40.21% (Fig. 2F), respectively. *In vitro* degradation assays demonstrated after 42 days of incubation, the degradation ratios of CG and CG-ASA were 73.05 ± 0.70% and 64.95 ± 1.26%, respectively, exhibiting highly similar degradation trends (Fig. 2G). Besides, CG and CG-ASA also possessed similarly remarkable compressive stress capabilities (Fig. 2H), which were far beyond those of the tetra-PEG hydrogel, revealing the importance of a rigid CS backbone to improve the mechanical strength of a composite gel. These data indicated that ASA loading did not alter the microarchitecture, swelling, degradation profiles, and mechanical performance of the CGs.

3.2. In Vitro ASA release profile of CG-ASA

Sustained-release of ASA would be conducive to maintaining an drug effective concentration in the scaffold for seeded cells; moreover, it might exert enduring anti-inflammatory effects on the surrounding tissue. The cumulative release curve demonstrated that ASA release exhibited an initial burst within 24 h, representing about 15% of the total. The release rate of ASA gradually decreased with extended time, and the cumulative release of aspirin was about 70% at 14 d (Fig. 2I).

3.3. Cytotoxicity and biocompatibility of CG-ASA

CCK-8 assays and live/dead staining were used to assess CG cytotoxicity toward PDLSCs. As shown in Fig. 3A, compared with the NC group, PDLSC viability was markedly elevated in the CG group after 24 and 48 h of incubation ($p < 0.05$, $p < 0.001$, respectively), implying that the CG scaffold was capable of stimulating PDLSCs propagation. Meanwhile, the cell viabilities of the CG-ASA group at 24, 48, and 72 h were significantly higher than those of the other two groups ($p < 0.05$, $p < 0.001$, $p < 0.01$, respectively). Intriguingly, at 72 h, CG-ASA could still promote PDLSC proliferation, while NC group caught up with CG group. This might be attributed to ASA supplementation. At 120 h, the effect of CS-ASA on PDLSCs proliferation disappeared, and the difference between groups was not statistically significant. PDLSCs live/dead assays showed that live PDLSCs appeared to be spindle-shaped with numerous filopodia. Bright green fluorescence showed strong cell viability, and dead cells were extremely rare among the three groups at the four different timepoints over two weeks (Fig. 3B). No distinguishable disparities in cell status were observed. The CCK-8 and cell live/dead staining results indicated neither of CG nor CG-ASA exhibited obvious cytotoxicity towards PDLSCs.

3.4. CG-ASA enhanced PDLSC osteogenic differentiation in Vitro

Excellent biocompatibility is a prerequisite for qualified cell carriers. Ideal scaffolds for bone tissue engineering should also boost progenitor cell osteogenic differentiation [5]. ALP and ARS staining and qRT-PCR were used to determine the osteoinductivity of CG-ASA. As shown in Fig. 4A, ALP and ARS staining revealed that compared with the other three groups, the CG-ASA group displayed the greatest staining intensity and ratios of positively stained areas ($p < 0.05$). These results suggested 7-day ALP activity and 14-day mineralized nodules were significantly augmented by CG-ASA. Relative mRNA expressions of osteogenic marker genes, including *RUNX2* (encoding RUNX family transcription factor 2), *ALP*, and *OCN* (encoding osteocalcin), were analyzed at the early, middle, and late stages (Day 5, 7 and 10, respectively) of osteogenesis (Fig. 4B). The qRT-PCR results showed that compared with *RUNX2* expression in the in NC group, its expression was increased significantly in the PEG-ASA and CG-ASA group at all time points ($^{**}p < 0.01$, $^{***}p < 0.001$). *ALP* expression was significantly upregulated at all time points ($^{*}p < 0.05$, $^{**}p < 0.01$, $^{***}p < 0.001$), while *OCN* was upregulated after day 7 ($^{*}p < 0.05$, $^{**}p < 0.01$, $^{***}p < 0.001$), implying that ASA-laden tetra-PEG hydrogel (PEG-ASA) scaffolds were capable of promoting PDLSCs osteogenic differentiation *in vitro*. Intriguingly, most of the bar charts in Fig. 4B show that expression of osteogenic markers increased more significantly in the CS-ASA group than that in the PEG-ASA group, revealing the beneficial promotion of cell adhesion and differentiation by CS components. These results indicated that CG-ASA was a promising scaffold to enhance PDLSC osteogenic differentiation *in vitro*.

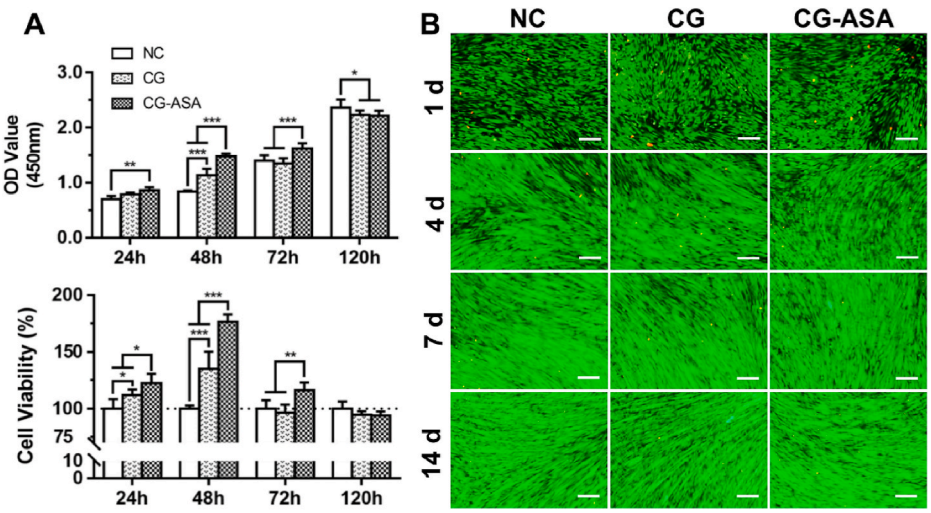

Fig. 3. Cytotoxicity of CGs *in vitro*. (A) CCK-8 assay of PDLSC proliferation and viability after co-culture for 24, 48, 72, and 120 h. (B) Live/dead staining of PDLSCs at specific time points (Day 1, 4, 7, and 14) in 2-weeks of co-culture. Calcein AM staining (green) shows strong viability of cells, EthD-1 labelling (red) shows dead cells. Scale bar = 500 μm. NC, negative control (*$p < 0.05$, **$p < 0.01$, ***$p < 0.001$). CG, composite gel; CCK-8, cell counting kit-8; PDLSCs, periodontal ligament stem cells.

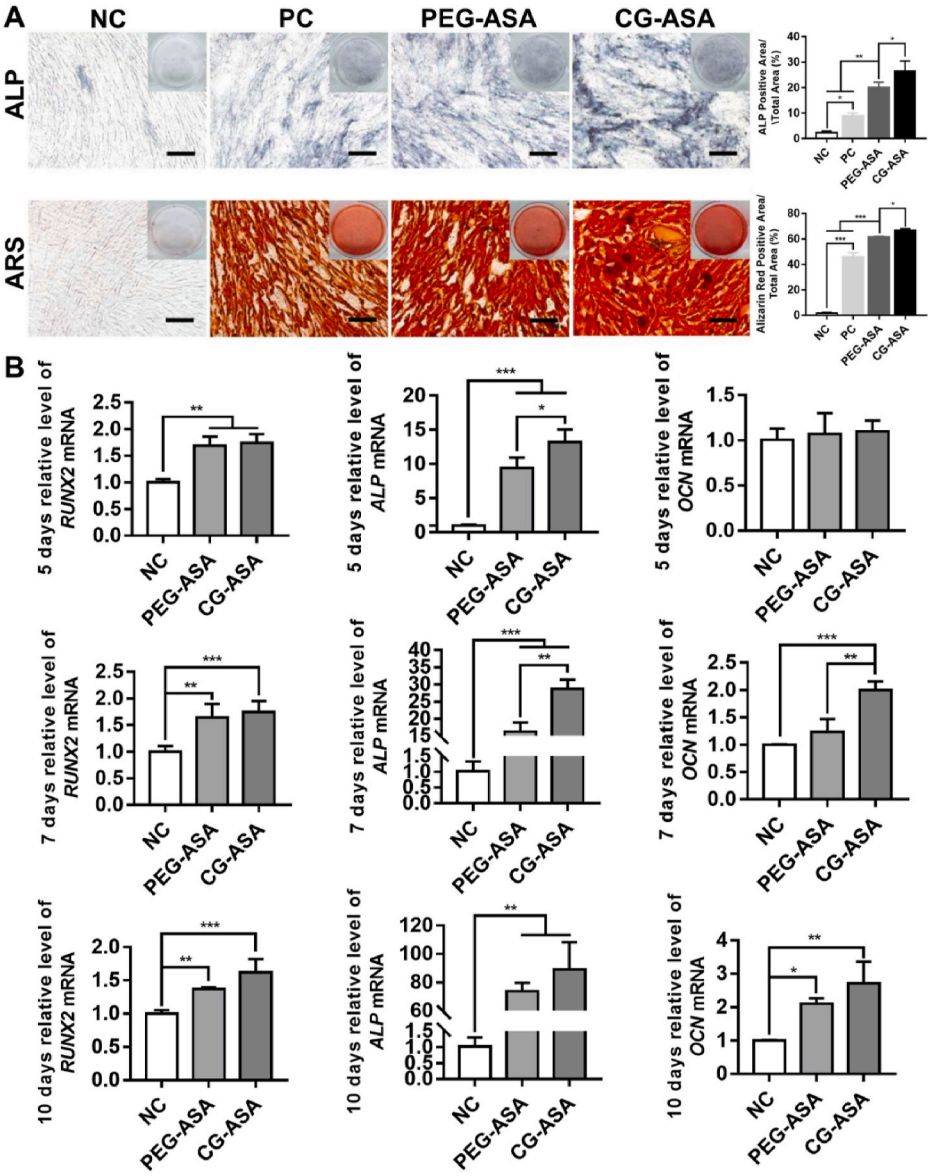

Fig. 4. Osteogenic potential of PDLSCs co-cultured with ASA-laden tetra-PEG gel and CG *in vitro*. (A) Gross-micrographs and semi-quantitative analysis of ALP and ARS staining. Scale bar = 200 μm. PC, positive control, PDLSCs were cultured with ODM. (B) PDLSCs relative mRNA expression of *RUNX2*, *ALP*, and *OCN* at the corresponding time points (*$p < 0.05$, **$p < 0.01$, ***$p < 0.001$). CG, composite gel; PDLSCs, periodontal ligament stem cells; ASA, acetylsalicylic acid; PEG, polyethylene glycol; ALP, alkaline phosphatase; ARS, Alizarin Red S; ODM, osteogenic differentiation medium; RUNX2, RUNX family transcription factor 2; OCN, osteocalcin.

3.5. CG-ASA increased the secretion of MCP-1 by PDLSCs, leading to macrophage M2 polarization

We established a mouse calvarial bone critical-sized defect model to examine the CGs' *in situ* osteogenic ability *in vivo*. The surface topography of PDLSCs-loaded CG complexes was observed by SEM after incubation for 48 h. PDLSCs appeared to be round-shaped and dispersed in the wrinkles and pores of the CGs (Fig. S2). Full-thickness calvarial bone defects (3 mm) were prepared and the corresponding sized CGs were implanted *in situ* (Fig. 5A). At 8 weeks after surgery, neo-bone formation was observed in all five groups *via* micro-CT (Fig. 5B–F). The BV/TV data showed that in the NC group, no observable newly-formed bone tissue had been formed (Fig. 5G). Compared with that in the CG group (1.48 ± 0.57%), the bone formation of the CG + PDLSCs group (7.31 ± 1.16%) and CG-ASA group (11.96 ± 2.07%) were greater, yet only the CG-ASA group showed a significant difference. By contrast, the CG-ASA + PDLSCs group (19.84 ± 1.99%) exhibited the highest rate of osteogenesis among all the groups, and the differences were statistically significant ($p < 0.05$). H&E staining (Fig. 5H) showed that the CG-ASA + PDLSCs group had the maximum bone regeneration in the defect areas, whereas the CG + PDLSCs group and CG-ASA group acquired less regenerated bone around the margins. Most of the defect areas in the CG group were filled with fibrous connective tissue. The microstructures of the newly-formed bone were relatively ordered and osteocytes were distributed more uniformly in the CG-ASA + PDLSCs group compared with that in the other three groups. Masson trichrome staining revealed that conspicuously more mature neo-bone was attained in the CG-ASA + PDLSCs group compared with that in the CG-ASA group. The latter evidently had much more blue-stained areas indicating immature collagen fibers and osteoid. The CG + PDLSCs and CG groups had identical staining characteristics.

To explain the underlying mechanisms of PDLSCs-laden CG-ASA-mediated osteogenesis, a series of prominent osteoimmune factors were tested at the transcriptional level. We found out that *MCP*-1 mRNA was predominantly upregulated in PDLSCs co-cultured with CG-ASA for 3 days (Fig. 6A, $p < 0.01$). To confirm this alteration, ELISA of MCP-1 was conducted at day 1, 4, and 7 (Fig. 6B). The results showed that PDLSCs in the CG-ASA + PDLSCs group secreted 908.7 ± 17.3, 759.7 ± 9.3, and 907.2 ± 5.1 pg/mL of MCP-1 into the supernatant at day 1, 4, 7, respectively, which was significantly higher than that in the empty CG group (775.0 ± 10.9, 689.4 ± 5.8, and 845.0 ± 8.8 pg/mL, respectively) and the NC group (758.3 ± 5.6l, 739.1 ± 21.3, and 815.4 ± 26.7 pg/mL, respectively. $^{*}p < 0.05$,$^{***}p < 0.001$). These results revealed that PDLSCs MCP-1 expression was significantly upregulated during co-culturing with CG-ASA *in vitro*. Thus, we hypothesized that CG-ASA upregulated PDLSC and host MSC MCP-1 expression and further

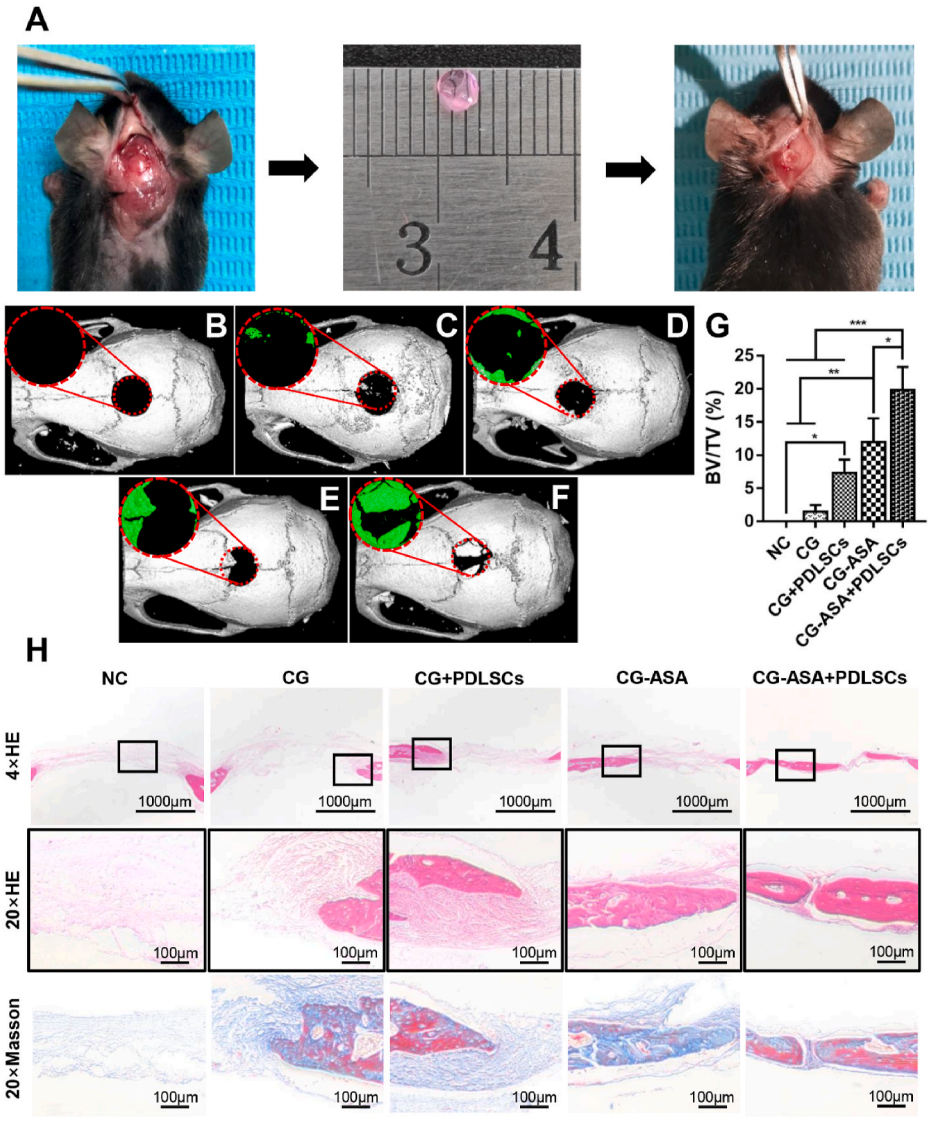

Fig. 5. PDLSCs-loaded CG-ASA promoted osteogenesis *in vivo*. (A) Surgical procedures for PDLSCs-CG complex implantation. Micro-CT 3D reconstruction images of mice calvarial bone defects implanted with (B) negative control (NC), (C) CG, (D) PDLSCs-loaded CG, (E) CG-ASA, and (F) PDLSCs-loaded CG-ASA after surgery for 8 weeks. (G) BV/TV, (H) HE staining and Masson trichrome staining of each group is shown ($^{*}p < 0.05$, $^{**}p < 0.01$, $^{***}p < 0.001$). CG, composite gel; PDLSCs, periodontal ligament stem cells; ASA, acetylsalicylic acid; CT, computed tomography; BV/TV, bone volume/total volume; HE, hematoxylin and eosin.

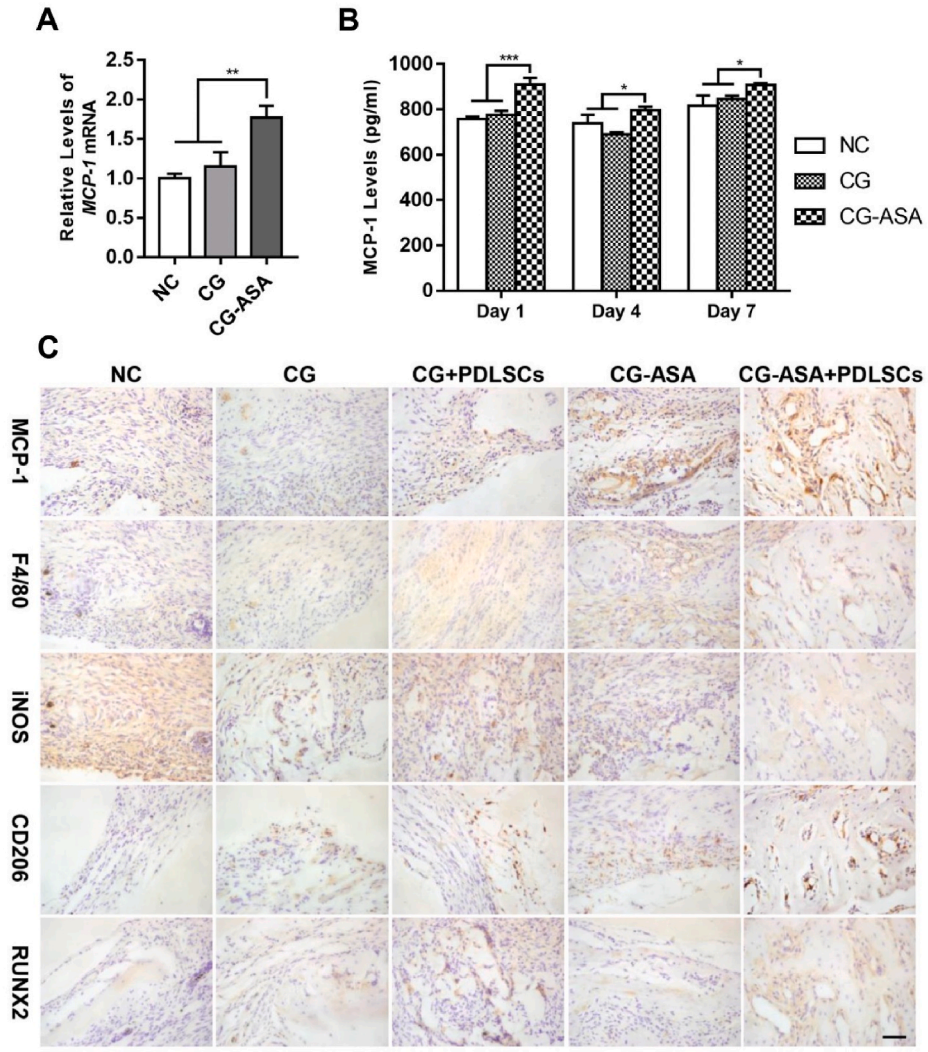

Fig. 6. PDLSCs-loaded CG-ASA promoted macrophage M2 polarization to achieve calvarial bone regeneration in mice. PDLSCs *in vitro* relative mRNA expression (A) and ELISA (B) of MCP-1 in the negative control (NC), CG, and CG-ASA groups at different timepoints. (*$p < 0.05$, **$p < 0.01$, ***$p < 0.001$). (C) Representative immunohistochemistry staining of MCP-1, F4/80, iNOS, CD206 and RUNX2. F4/80^{+}iNOS^{+} cells represent M1 macrophages, while F4/80^{+}CD206^{+} cells represent M2 macrophages. Scale bar, 50 μm. NC, negative control; CG, composite gel; PDLSCs, periodontal ligament stem cells; ASA, acetylsalicylic acid; ELISA, enzyme-linked immunosorbent assay; MCP-1, monocyte chemoattractant protein-1; iNOS, inducible NO synthase.

promoted macrophage M2 polarization. In the early phase of bone repair procedure (2 weeks after implantation), compared with NC, CG and CG + PDLSCs group, IHC staining showed a significant elevation of MCP-1 in CG-ASA and PDLSC-laden CG-ASA group at the defect sites, which confirmed our *in vitro* results (Fig. 6C). Moreover, the numbers of F4/80^{+}CD206^{+} cells increased dramatically, while F4/80^{+}iNOS^{+} cells decreased in CG + PDLSCs, CG-ASA and CG-ASA + PDLSCs group, which might be attribute to exogenic PDLSCs regulation sustained release of ASA or synergistic effect of both factors. As an early marker of bone regeneration, RUNX2 was stained to determine the initiation of bone formation. RUNX2 positive cell numbers were increased in CG + PDLSCs, CG-ASA and CG-ASA + PDLSCs group, which were in accordance with the rise of MCP-1, M2 macrophage levels and the *in vivo* osteogenesis in these groups, indicating the underlying mechanism of present study might be related to MCP-1 secretion and macrophage M2 polarization.

4. Discussion

With the aim of better simulating the process of physiological bone repair and building a “bone-friendly” microenvironment, biomimetic scaffolds showing sustained release of bioactive factors have become a conventional strategy in BTE [33,34]. CS is an appealing natural basic polysaccharide for TERM because of its remarkable hydrophilicity and biocompatibility. It has been widely reported that CS is capable of promoting cell proliferation and wound healing, and abating local inflammatory responses [35,36]. As early as 2000, Park et al. [37] constructed platelet derived growth factor (PDGF)-loaded CS scaffolds for rat calvarial bone tissue regeneration, and verified this construct as a BTE scaffold. Bernardi and co-workers demonstrated that CS-based scaffolds acted as an independent stimulus for osteogenic differentiation, rather than merely acting as a cell container [38]. However, pure CS hydrogel is relatively brittle and tends to degrade *in vivo*. Thus, researchers often incorporated rigid CS into other synthesized hydrogels or inorganic components to enhance their mechanical properties. In the present study, we established tetra-PEG-CS composite gel scaffolds. Tetra-PEG hydrogel proved to be mechanically tough, and thus has been used as a sealant for visceral hemostasis [39]. Our *in vitro* osteogenesis experiments demonstrated that CG-ASA had more reliable outcomes than PEG-ASA, suggesting that CS introduction had beneficial effects on MSC osteogenic differentiation.

In the physiological process of bone healing, bioactive factors are orchestrated in a spatiotemporal manner, some of which are secreted continuously or released from extracellular matrix storage to prolong osteogenic effects. For drug-laden BTE scaffolds, the burst release and uncontrolled diffusion of physically-encapsulated small hydrophilic drugs will lead to latent detrimental effects, e.g., a high local drug concentration, cytotoxicity, and even tumorigenesis [40]. If a drug is tethered by covalent bonds, the release kinetics are mainly dependent on the stability of those chemical bonds. Thus, the release rate will be

dramatically reduced; however, the chemical linkages might alter the drug's biochemical activity and efficiency. Previous studies have shown that the introduction of electrostatic interactions between the carrier and the drug molecules can significantly improve the drug release kinetics without changing the chemical structure [41,42]. In the present study, aspirin was immobilized via physical entrapment in polymer networks and by electrostatic interaction between the drug molecules and the CS chains in the CG scaffold. In contrast to our previous study [43], the ASA release curve was notably gentler. This might be ascribed to electrostatic interaction or the synergist effects of electrostatic interaction and physical encapsulation. The *in vivo* results revealed that CG-ASA treatment induced a larger amount of neo-bone than treatment with empty CG, regardless of whether PDLSCs were incorporated or not, implying that sustained release of ASA might be an independent factor that stimulates mouse calvarial bone regeneration.

Autologous MSCs are not likely to trigger a host immune response and therefore will differentiate into osteoblasts and deposit bone directly. However, sources of autologous MSCs are limited, and in addition, the aberrant hormones, inflammation, and metabolic environment will impair the proliferation, differentiation, and immunomodulation of host MSCs [44,45]. Therefore, it is always not feasible to obtain a satisfactory osteogenic effect by transplanting autologous MSCs. Although MSCs possess low immunogenicity, some studies reported that allogeneic or xenogeneic MSCs would still be eliminated over the long term [19,46], while their therapeutic effects persisted, which might be explained by host cell reprogramming [47] after phagocytosis, which would ameliorate local immune microenvironments. Substantial research has revealed that xenogeneic MSCs have certain effects of immunoregulation [48]. In the present study, CG-ASA incorporating PDLSCs obtained the maximum bone regeneration among all the groups. Moreover, in contrast to the CG-ASA group, the CG-ASA + PDLSCs group possessed the best histological structure in terms of new bone formation. These observations suggested that xenogeneic PDLSCs might play a crucial role in mice calvarial bone regeneration.

Biomimetic scaffolds could promote bone tissue regeneration *via* biomaterial-mediated regulation of macrophage polarization. MCP-1, also known as CC chemokine ligand 2 (CCL2), is secreted by various types of cells, including MSCs, under inflammatory stimulus. Accumulating evidence indicates that MCP-1 plays crucial roles in muscle and cartilage regeneration after injury [49,50]. Besides being a potent chemoattractant for monocyte-macrophage lineage cells, MCP-1 also promotes macrophage M2 polarization, thus alleviating bone resorption caused by periodontitis [51] and promoting bone regeneration [52,53]. Herein, under the sustained *in vitro* stimulation of CG-ASA, the expression of PDLSC and host MSC *MCP-1* was upregulated significantly. Our IHC results preliminarily demonstrated that CG-ASA recruited macrophages to the defect areas and promoted M2 polarization. We surmised that the underlying mechanism of CG-mediated bone regeneration might be related to upregulation of MCP-1, which led to macrophage M2 polarization. This hypothesis should be verified in future studies.

Helms and Schneider believed that the mechanisms of cranial skeleton regeneration are distinctive from those of long bones [54]. The seeded cells used in this study, PDLSCs, are highly homologous to the progenitors that form craniofacial tissues, and thus PDLSCs might be beneficially applied to promote bone regeneration in craniomaxillofacial areas. To date, bioactive materials for bone regenerative medicine have not yet been fully translated to clinical use because of their poor cost-effectiveness and intricate manufacturing procedures [55]. As a prospective candidate scaffold for future BTE, the raw materials of CG-ASA can be simply obtained and the fabrication process is relatively easy, which are important prerequisites for further clinical translation. Thus, we believe that these PDLSCs-incorporated CG-ASA scaffolds represent a promising alternative clinical intervention for craniofacial bone loss resulting from trauma, maxillofacial surgery, or infection diseases. Thus, our results warrant additional translational investigations in future studies.

5. Conclusion

In summary, we developed a novel tetra-PEG-CS composite gel for bone tissue engineering. The uniform tetra-PEG network offered a satisfactory pore size and mechanical behavior, while the rigid CS contributed to the excellent cell compatibility. After *in situ* encapsulation of ASA molecules via electrostatic interactions, *in vitro* studies showed this biocompatible CG-ASA displayed sustained-release of ASA over 14 days. The CG-ASA favored PDLSCs culture, cell-affinity, and proliferation, and thus exhibited superb osteogenesis augmentation. The underlying mechanism *in vivo* might be ascribed to the sustained release of ASA and MCP-1-mediated M2 macrophage recruitment and polarization. The simplicity of the process and the widely tunable properties of the composite hydrogels make them promising candidates for biomedical applications in cell therapy, drug delivery, and tissue engineering.

CRediT authorship contribution statement

Yunfan Zhang: Conceptualization, Investigation, Methodology, Validation, Funding acquisition, Writing – original draft. **Xueyu Dou:** Conceptualization, Investigation, Methodology, Validation. **Lingyun Zhang:** Conceptualization, Investigation, Methodology, Validation. **Hufei Wang:** Conceptualization, Investigation, Methodology, Validation. **Ting Zhang:** Investigation, Methodology, Validation. **Rushui Bai:** Investigation, Methodology, Validation. **Qiannan Sun:** Investigation, Methodology, Validation. **Xing Wang:** Conceptualization, Methodology, Supervision. **Tingting Yu:** Validation, Conceptualization, Funding acquisition, Supervision, Writing – review & editing. **Decheng Wu:** Supervision, Conceptualization. **Bing Han:** Conceptualization, Funding acquisition, Writing – review & editing. **Xuliang Deng:** Supervision, Conceptualization.

Declaration of competing interest

The authors declare no conflict of interest.

Acknowledgment

This work is supported by the National Key R&D Program of China (2020YFA0710401), National Natural Science Foundation of China (51972005, 51903003, 51973226, 81871782 and 51672009) and the Youth Innovation Promotion Association CAS (No. 2019031) for financial support.

Appendix A. Supplementary data

Supplementary data to this article can be found online at https://doi.org/10.1016/j.bioactmat.2021.09.033.

References

[1] G.M. Crane, S.L. Ishaug, A.G. Mikos, Bone tissue engineering, Nat. Med. 1 (12) (1995) 1322–1324.
[2] R.F. Service, Tissue engineers build new bone, Science 289 (5484) (2000) 1498–1500.
[3] K. Zhang, Y. Zhou, C. Xiao, W. Zhao, H. Wu, J. Tang, Z. Li, S. Yu, X. Li, L. Min, Z. Yu, G. Wang, L. Wang, K. Zhang, X. Yang, X. Zhu, C. Tu, X. Zhang, Application of hydroxyapatite nanoparticles in tumor-associated bone segmental defect, Sci Adv 5 (8) (2019), eaax6946.
[4] R. Langer, J.P. Vacanti, Tissue engineering, Science 260 (5110) (1993) 920–926.
[5] Z. Zou, L. Wang, Z. Zhou, Q. Sun, D. Liu, Y. Chen, H. Hu, Y. Cai, S. Lin, Z. Yu, B. Tan, W. Guo, Z. Ling, X. Zou, Simultaneous incorporation of PTH(1-34) and nano-hydroxyapatite into Chitosan/Alginate Hydrogels for efficient bone regeneration, Bioact Mater 6 (6) (2021) 1839–1851.
[6] S.J. Wang, D. Jiang, Z.Z. Zhang, Y.R. Chen, Z.D. Yang, J.Y. Zhang, J. Shi, X. Wang, J.K. Yu, Biomimetic Nanosilica-collagen scaffolds for in situ bone regeneration: toward a cell-free, one-step surgery, Adv. Mater. 31 (49) (2019), e1904341.
[7] L. Claes, S. Recknagel, A. Ignatius, Fracture healing under healthy and inflammatory conditions, Nat. Rev. Rheumatol. 8 (3) (2012) 133–143.

[8] P.M. Mountziaris, P.P. Spicer, F.K. Kasper, A.G. Mikos, Harnessing and modulating inflammation in strategies for bone regeneration, Tissue Eng. B Rev. 17 (6) (2011) 393–402.
[9] N.J. Horwood, Macrophage polarization and bone formation: a review, Clin. Rev. Allergy Immunol. 51 (1) (2016) 79–86.
[10] M. Bartneck, K.H. Heffels, Y. Pan, M. Bovi, G. Zwadlo-Klarwasser, J. Groll, Inducing healing-like human primary macrophage phenotypes by 3D hydrogel coated nanofibres, Biomaterials 33 (16) (2012) 4136–4146.
[11] J. Lee, H. Byun, S.K. Madhurakkat Perikamana, S. Lee, H. Shin, Current advances in immunomodulatory biomaterials for bone regeneration, Adv Healthc Mater 8 (4) (2019), e1801106.
[12] O.R. Mahon, D.C. Browe, T. Gonzalez-Fernandez, P. Pitacco, I.T. Whelan, S. Von Euw, C. Hobbs, V. Nicolosi, K.T. Cunningham, K.H.G. Mills, D.J. Kelly, A. Dunne, Nano-particle mediated M2 macrophage polarization enhances bone formation and MSC osteogenesis in an IL-10 dependent manner, Biomaterials 239 (2020), 119833.
[13] I. Cockerill, Y. Su, J.H. Lee, D. Berman, M.L. Young, Y. Zheng, D. Zhu, Micro-/Nanotopography on Bioresorbable Zinc dictates cytocompatibility, bone cell differentiation, and macrophage polarization, Nano Lett. 20 (6) (2020) 4594–4602.
[14] Y. Liu, L. Wang, T. Kikuiri, K. Akiyama, C. Chen, X. Xu, R. Yang, W. Chen, S. Wang, S. Shi, Mesenchymal stem cell-based tissue regeneration is governed by recipient T lymphocytes via IFN-gamma and TNF-alpha, Nat. Med. 17 (12) (2011) 1594–1601.
[15] Y. Cao, J. Xiong, S. Mei, F. Wang, Z. Zhao, S. Wang, Y. Liu, Aspirin promotes bone marrow mesenchymal stem cell-based calvarial bone regeneration in mini swine, Stem Cell Res. Ther. 6 (2015) 210.
[16] Y. Liu, C. Chen, S. Liu, D. Liu, X. Xu, X. Chen, S. Shi, Acetylsalicylic acid treatment improves differentiation and immunomodulation of SHED, J. Dent. Res. 94 (1) (2015) 209–218.
[17] T. Yu, B. Yan, J. Li, T. Zhang, R. Yang, X. Wang, Y. Liu, D. Liu, Acetylsalicylic acid rescues the immunomodulation of inflamed gingiva-derived mesenchymal stem cells via upregulating FasL in mice, Stem Cell Res. Ther. 10 (1) (2019) 368.
[18] B.-M. Seo, M. Miura, S. Gronthos, P. Mark Bartold, S. Batouli, J. Brahim, M. Young, P. Gehron Robey, C.Y. Wang, S. Shi, Investigation of multipotent postnatal stem cells from human periodontal ligament, Lancet 364 (9429) (2004) 149–155.
[19] G.T.J. Huang, S. Gronthos, S. Shi, Mesenchymal stem cells derived from dental tissuesvs. Those from other sources: their biology and role in regenerative medicine, J. Dent. Res. 88 (9) (2009) 792–806.
[20] D. Seliktar, Designing cell-compatible hydrogels for biomedical applications, Science 336 (6085) (2012) 1124–1128.
[21] N. Gjorevski, N. Sachs, A. Manfrin, S. Giger, M.E. Bragina, P. Ordonez-Moran, H. Clevers, M.P. Lutolf, Designer matrices for intestinal stem cell and organoid culture, Nature 539 (7630) (2016) 560–564.
[22] S. Stratton, N.B. Shelke, K. Hoshino, S. Rudraiah, S.G. Kumbar, Bioactive polymeric scaffolds for tissue engineering, Bioact Mater 1 (2) (2016) 93–108.
[23] T. Sakai, Y. Akagi, T. Matsunaga, M. Kurakazu, U.I. Chung, M. Shibayama, Highly elastic and deformable hydrogel formed from tetra-arm polymers, Macromol. Rapid Commun. 31 (22) (2010) 1954–1959.
[24] P.B. Malafaya, G.A. Silva, R.L. Reis, Natural-origin polymers as carriers and scaffolds for biomolecules and cell delivery in tissue engineering applications, Adv. Drug Deliv. Rev. 59 (4–5) (2007) 207–233.
[25] M.M. Islam, M. Shahruzzaman, S. Biswas, M. Nurus Sakib, T.U. Rashid, Chitosan based bioactive materials in tissue engineering applications-A review, Bioact Mater 5 (1) (2020) 164–183.
[26] Z. Shen, S. Kuang, Y. Zhang, M. Yang, W. Qin, X. Shi, Z. Lin, Chitosan hydrogel incorporated with dental pulp stem cell-derived exosomes alleviates periodontitis in mice via a macrophage-dependent mechanism, Bioact Mater 5 (4) (2020) 1113–1126.
[27] L. Bugnicourt, C. Ladaviere, A close collaboration of chitosan with lipid colloidal carriers for drug delivery applications, J. Contr. Release 256 (2017) 121–140.
[28] L.K. Meena, P. Raval, D. Kedaria, R. Vasita, Study of locust bean gum reinforced cyst-chitosan and oxidized dextran based semi-IPN cryogel dressing for hemostatic application, Bioact Mater 3 (3) (2018) 370–384.
[29] K.J. Livak, T.D. Schmittgen, Analysis of relative gene expression data using real-time quantitative PCR and the 2(-Delta Delta C(T)) Method, Methods 25 (4) (2001) 402–408.
[30] T.T. Yu, F.Z. Cui, Q.Y. Meng, J. Wang, D.C. Wu, J. Zhang, X.X. Kou, R.L. Yang, Y. Liu, Y.S. Zhang, F. Yang, Y.H. Zhou, Influence of surface chemistry on adhesion and osteo/odontogenic differentiation of dental pulp stem cells, ACS Biomater. Sci. Eng. 3 (6) (2017) 1119–1128.
[31] Z.K. Cui, S. Kim, J.J. Baljon, B.M. Wu, T. Aghaloo, M. Lee, Microporous methacrylated glycol chitosan-montmorillonite nanocomposite hydrogel for bone tissue engineering, Nat. Commun. 10 (1) (2019) 3523.
[32] S.S. Jin, D.Q. He, D. Luo, Y. Wang, M. Yu, B. Guan, Y. Fu, Z.X. Li, T. Zhang, Y. H. Zhou, C.Y. Wang, Y. Liu, A biomimetic hierarchical Nanointerface orchestrates macrophage polarization and mesenchymal stem cell recruitment to promote endogenous bone regeneration, ACS Nano 13 (6) (2019) 6581–6595.
[33] S.H. Lee, H. Shin, Matrices and scaffolds for delivery of bioactive molecules in bone and cartilage tissue engineering, Adv. Drug Deliv. Rev. 59 (4–5) (2007) 339–359.
[34] M. Farokhi, F. Mottaghitalab, M.A. Shokrgozar, K.L. Ou, C. Mao, H. Hosseinkhani, Importance of dual delivery systems for bone tissue engineering, J. Contr. Release 225 (2016) 152–169.
[35] I. Bano, M. Arshad, T. Yasin, M.A. Ghauri, M. Younus, Chitosan: a potential biopolymer for wound management, Int. J. Biol. Macromol. 102 (2017) 380–383.
[36] I. Fasolino, M.G. Raucci, A. Soriente, C. Demitri, M. Madaghiele, A. Sannino, L. Ambrosio, Osteoinductive and anti-inflammatory properties of chitosan-based scaffolds for bone regeneration, Mater Sci Eng C Mater Biol Appl 105 (2019), 110046.
[37] Y.J. Park, Y.M. Lee, S.N. Park, S.Y. Sheen, C.P. Chung, S.J. Lee, Platelet derived growth factor releasing chitosan sponge for periodontal bone regeneration, Biomaterials 21 (2) (2000) 153–159.
[38] S. Bernardi, F. Re, K. Bosio, K. Dey, C. Almici, M. Malagola, P. Guizzi, L. Sartore, D. Russo, Chitosan-hydrogel polymeric scaffold Acts as an independent primary inducer of osteogenic differentiation in human mesenchymal stromal cells, Materials 13 (16) (2020).
[39] Y. Bu, L. Zhang, G. Sun, F. Sun, J. Liu, F. Yang, P. Tang, D. Wu, Tetra-PEG based hydrogel sealants for in vivo visceral hemostasis, Adv. Mater. 31 (28) (2019), e1901580.
[40] D. de Melo Pereira, P. Habibovic, Biomineralization-inspired material design for bone regeneration, Adv Healthc Mater 7 (22) (2018), e1800700.
[41] E. Mauri, G.M.F. Chincarini, R. Rigamonti, L. Magagnin, A. Sacchetti, F. Rossi, Modulation of electrostatic interactions to improve controlled drug delivery from nanogels, Mater Sci Eng C Mater Biol Appl 72 (2017) 308–315.
[42] S. Choi, J.S. Lee, J. Shin, M.S. Lee, D. Kang, N.S. Hwang, H. Lee, H.S. Yang, S. W. Cho, Osteoconductive hybrid hyaluronic acid hydrogel patch for effective bone formation, J. Contr. Release 327 (2020) 571–583.
[43] Y. Zhang, N. Ding, T. Zhang, Q. Sun, B. Han, T. Yu, A tetra-PEG hydrogel based aspirin sustained release system exerts beneficial effects on periodontal ligament stem cells mediated bone regeneration, Front Chem 7 (2019) 682.
[44] R.J. Cheng, A.J. Xiong, Y.H. Li, S.Y. Pan, Q.P. Zhang, Y. Zhao, Y. Liu, T.N. Marion, Mesenchymal stem cells: allogeneic MSC may Be immunosuppressive but autologous MSC are dysfunctional in lupus patients, Front Cell Dev Biol 7 (2019) 285.
[45] B.D. Sui, C.H. Hu, C.X. Zheng, Y. Jin, Microenvironmental views on mesenchymal stem cell differentiation in aging, J. Dent. Res. 95 (12) (2016) 1333–1340.
[46] T.S. de Windt, L.A. Vonk, I.C.M. Slaper-Cortenbach, R. Nizak, M.H.P. van Rijen, D. B.F. Saris, Allogeneic MSCs and recycled autologous chondrons mixed in a one-stage cartilage cell transplantion: a first-in-man trial in 35 patients, Stem Cell. 35 (8) (2017) 1984–1993.
[47] R.E. Voll, M. Herrmann, E.A. Roth, C. Stach, J.R. Kalden, I. Girkontaite, Immunosuppressive effects of apoptotic cells, Nature 390 (6658) (1997) 350–351.
[48] D.J. Prockop, J.Y. Oh, R.H. Lee, Data against a common Assumption: xenogeneic mouse models can Be used to assay suppression of immunity by human MSCs, Mol. Ther. 25 (8) (2017) 1748–1756.
[49] H. Lu, D. Huang, R.M. Ransohoff, L. Zhou, Acute skeletal muscle injury: CCL2 expression by both monocytes and injured muscle is required for repair, Faseb. J. 25 (10) (2011) 3344–3355.
[50] C.L. Jablonski, C. Leonard, P. Salo, R.J. Krawetz, CCL2 but not CCR2 is required for spontaneous Articular cartilage regeneration post-injury, J. Orthop. Res. 37 (12) (2019) 2561–2574.
[51] Z. Zhuang, S. Yoshizawa-Smith, A. Glowacki, K. Maltos, C. Pacheco, M. Shehabeldin, M. Mulkeen, N. Myers, R. Chong, K. Verdelis, G.P. Garlet, S. Little, C. Sfeir, Induction of M2 macrophages prevents bone loss in murine periodontitis models, J. Dent. Res. 98 (2) (2019) 200–208.
[52] X. Sun, Z. Ma, X. Zhao, W. Jin, C. Zhang, J. Ma, L. Qiang, W. Wang, Q. Deng, H. Yang, J. Zhao, Q. Liang, X. Zhou, T. Li, J. Wang, Three-dimensional bioprinting of multicell-laden scaffolds containing bone morphogenic protein-4 for promoting M2 macrophage polarization and accelerating bone defect repair in diabetes mellitus, Bioact Mater 6 (3) (2021) 757–769.
[53] Y. Niu, Z. Wang, Y. Shi, L. Dong, C. Wang, Modulating macrophage activities to promote endogenous bone regeneration: biological mechanisms and engineering approaches, Bioact Mater 6 (1) (2021) 244–261.
[54] J.A. Helms, R.A. Schneider, Cranial skeletal biology, Nature 423 (6937) (2003) 326–331.
[55] D. Tang, R.S. Tare, L.Y. Yang, D.F. Williams, K.L. Ou, R.O. Oreffo, Biofabrication of bone tissue: approaches, challenges and translation for bone regeneration, Biomaterials 83 (2016) 363–382.